Lawrence Berkeley National Laboratory

Title
An intrinsic peak-dip-hump and strong coupling effects in $Bi_{2}Sr_{2}CaCu_{2}O_{8+\delta}$ ARPES data near $(\pi,0)$

Permalink
https://escholarship.org/uc/item/18h0c8q1

Authors
Gromko, AD
Chuang, Y-D
Fedorov, AV
et al.

Publication Date
2002-05-17

Peer reviewed

An intrinsic peak-dip-hump and strong coupling effects in
$Bi_2Sr_2CaCu_2O_{8+\delta}$ ARPES data near $(\pi,0)$

A. D. Gromko[1], Y.-D. Chuang[1,2], A. V. Fedorov[1,2], Y. Aiura[3], Y. Yamaguchi[3], K. Oka[3], Yoichi Ando[4], D. S. Dessau[1]

[1]*Department of Physics, University of Colorado, Boulder, Colorado 80309-0390*
[2]*Advanced Light Source, Lawrence Berkeley National Laboratory, Berkeley, CA 94720*
[3]*AIST, AIST Tsukuba Central 2, 1-1-1 Umezono, Tsukuba, Ibaraki 305-8568, Japan and*
[4]*CRIEPI, 2-11-1 Iwato-Kita, Komae, Tokyo 201-8511, Japan*
(Dated: May 8, 2018)

A well-known peak-dip-hump structure exists near $(\pi,0)$ in superconducting state ARPES spectra of $Bi_2Sr_2CaCu_2O_{8+\delta}$ (Bi2212). Here we report results on optimal and overdoped Bi2212 samples indicating the traditional peak-dip-hump structure observed near $(\pi,0)$ is largely due to bilayer splitting. However a separate, much weaker peak-dip-hump (PDH) structure distinct from bilayer splitting can be detected near $(\pi,0)$. This new PDH structure is consistent with electronic coupling to the magnetic resonance mode in Bi2212. Both the dispersion and line shape signatures indicate strong coupling to this mode.

The anomalies observed in the normal and superconducting-state electronic structure of the cuprates verify the complexity and richness of High-Temperature Superconductivity (HTS) [1]. Angle-resolved photoemission spectroscopy (ARPES) has proven to be an invaluable tool for advancing our understanding of HTS due to the energy and momentum-dependent information it provides. One of the most dissected features of ARPES spectra from the cuprate $Bi_2Sr_2CaCu_2O_{8+\delta}$ (Bi2212) has been the so-called peak-dip-hump (PDH) structure found in the superconducting state energy distribution curves (EDCs) near the $(\pi,0)$ point of the Brillouin zone. This structure consists of a sharp, low binding energy ($\sim 30meV$) peak, a broad high binding energy ($\sim 100meV$) hump, and a spectral dip between them [2, 3, 4, 5]. Similar structures are observed in tunnelling spectra from both HTSs [6, 7] and strongly-coupled conventional superconductors, where in the latter the PDH has been shown to match the phonon density of states measured in neutron scattering experiments [8]. The successful identification of electron-phonon coupling as the mechanism for conventional superconductivity increases the importance of understanding the PDH structure in HTSs.

In light of this, many well-known theories such as the marginal Fermi Liquid [9] and resonating valence bond interlayer tunnelling theories [10] have attempted to incorporate the PDH structure. More recently, it has been widely discussed in terms of coupling to some boson, with particular attention paid to the magnetic resonance mode observed in inelastic neutron scattering (INS) experiments [11]. One proposed connection between the INS and ARPES results relates the energy of the magnetic mode to the energy position of the dip [3, 4, 5]. Alternatively, other reports connect the weight of the sharp peak to a superfluid condensate fraction [12]. All of these ideas model a single, broad normal state peak replaced by the PDH structure in the superconducting state. However, recent advances in ARPES normal state data, namely

the detection of bilayer-band splitting (coupling between CuO_2 planes within a unit cell) [13, 14], show that the normal state spectra display both bonding (B) and anti-bonding (A) band features near $(\pi,0)$ instead of a single peak. With this new knowledge, it is natural to question the effect of bilayer splitting on the superconducting state spectra and the PDH [13, 14, 15]. Here we argue that the classical PDH structure observed near $(\pi,0)$ in Bi2212 is in fact an artifact of bilayer splitting. In addition, we report the first observations of a new PDH near $(\pi,0)$ contained within a single band. This new peak-dip-hump feature is argued to be intrinsic and of a lower energy scale and strength than the classical PDH. The strength of the dispersion kink associated with the new peak-dip-hump structure suggests strong electronic coupling.

The data presented here were taken at the Stanford Synchrotron Radiation Laboratory (SSRL), Stanford, and at the Advanced Light Source (ALS), Berkeley. At both facilities we used Scienta 200mm electron spectrometers, allowing the simultaneous collection of data along a $\sim 14°$ angular slice with 0.08° resolution along the slice. The beamline and analyzer slits were adjusted to achieve an experimental energy resolution of 12meV, as determined by the 10-90% width of a gold Fermi edge. The photon energy was tuned to 20eV, with the polarization along the $(0,0) - (\pi,0)$ direction. The analyzer slit direction was parallel to the $(0,0) - (\pi,0)$ direction for all cuts (see inset, figure 1) . We present data from Bi2212 samples at four doping levels: heavily overdoped OD58 ($T_c = 58K, \Delta T_c = 3K$) and OD71 ($T_c = 71K, \Delta T_c = 4K$), optimally doped OP91 ($T_c = 91K, \Delta T_c = 2K$), and lightly underdoped UD85 ($T_c = 85K, \Delta T_c = 6K$).

Figure 1(a)-(l) shows a sampling of raw data for OP91 and OD71 both above and below T_c, presented as false-color scale intensity plots. In general, two features are observed in each panel, which are lableled as the antibonding (A) and bonding (B) bands due to bilayer splitting.

Superstructure (SS) bands due to the lattice mismatch of the BiO and CuO_2 planes are occasionally seen as well. While bilayer splitting is well accepted for the overdoped regime of Bi2212 [13, 14, 15], the data in panels (k) and (l) are probably the clearest data to date demonstrating the persistence of bilayer splitting to lower doping levels where the instrinsic line broadening makes the deconvolution into separate features more difficult.

We now examine how bilayer splitting manifests itself in the EDC line shape along the well-studied $(0,0)-(\pi,0)$ symmetry line. Figures 1(m) and (n) show EDCs in both the normal and superconducting states along $(0,0) - (\pi,0)$. These curves are taken as vertical (energy) slices from the center cuts for OD71, and from cuts similar to and including those in panels (k) and (l) for OP91. The EDCs at both temperatures show two dominant spectral features, a low energy ($\sim 30meV$) sharp peak and a higher energy ($\sim 100meV$) broad hump. From panels (a)-(j), we see that the energy scales of the two features directly correspond to the A and B bands for sample OD71. Similar agreement is observed for the full data set on OP91, not shown here. From this agreement we deem the EDC line shape along $(0,0)-(\pi,0)$ to be a direct result of bilayer splitting rather than the signature of self-energy effects. In fact, recent studies indicate the intensities of the two EDC peaks vary independently with photon energy [15, 16]. Our temperature-dependent data in figure 1 is complimentary to these studies, since it shows the "classic" PDH structure is present in both the normal and superconducting states in both overdoped and optimally doped samples. Although at present the severe spectral broadening found in underdoped samples [17] disallows accurate temperature-dependent measurements of bilayer splitting, the aforementioned photon energy-dependent reports indicate bilayer splitting is present in the normal state of underdoped Bi2212 samples [16].

Although our data strongly indicates that the standard PDH structure at $(\pi,0)$ is due simply to bilayer splitting, there is a new PDH structure appearing in the superconducting state data near $(\pi,0)$ associated with a new energy scale E_{kink}. Kink effects have been discussed recently in ARPES studies of HTS's [5, 18, 19, 20], mostly connected with the nodal region and obtained from momentum distribution curve (MDC) data, as illustrated for UD85 in figure 2(a). We present underdoped data since in these samples the nodal kink or self-energy effects are strongest [18, 19, 20]. The temperature dependence of the nodal kink is very weak, as demonstrated by the similarity of the normal state (black dots) and superconducting state (red dots) MDC-derived dispersions. Figure 1 shows that the data near $(\pi,0)$ (for example panels (e) and (j)) has a more significant change in dispersion than the nodal data [18].

This can be more clearly seen in figure 2(b), which shows a blowup up of $k_y = 1.0\pi$ superconducting state data from sample OD58. On the graph we have traced a segment of the dispersion of the A and B bands, for which we have made use of both EDCs (black and blue dots) and MDCs (red dots) [21]. The possibility that the MDC and EDC peak positions do not match in the presence of self-energy effects has been pointed out in the literature [5, 22] and is especially clear in this data near the kink energy scale of $40meV$, shown by the horizontal blue line. While the kink energy scale shows up in the MDC-derived dispersion (red), it is even more clear in the EDC dispersion (blue), which asymptotically approaches the kink energy scale. In this instance, the disagreeing portions of the MDC and EDC dispersion represent the splitting of the B band dispersion into two branches. The low energy EDC dispersion tracks the renormalized part of the B band dispersion (B'), while at energies above E_{kink} the MDC dispersion tracks the unrenormalized part (B''). The EDC dispersion also roughly tracks B'' at binding energies below E_{kink}, however as shown in figure 2(c) these features are broad and hence the dispersion is not shown. Previously, from MDC data only, we argued that the detailed temperature, momentum, and doping dependence of the kink scale at $(\pi,0)$ indicate that this kink is clearly different from and stronger than the nodal kink, and that it is likely a result of electronic coupling to the magnetic resonance mode observed in inelastic neutron scattering [18]. Two branches can be understood in terms of coupling to a bosonic mode [3, 23], as only virtual excitations can be excited below E_{kink} while real ones which damp the system can be excited above E_{kink}. The peak intensities (related to the imaginary part of the self-energy) are also consistent with this, showing a large increase in spectral weight below E_{kink}.

We now show the new PDH in the EDCs due to the kink effect. At $k_x = 0.1\pi$ (figure 2(c)), the normal state EDC basically shows one broad feature cut by the Fermi function, which we now know to be a superimposition of the A and B bands. As the sample goes superconducting, the EDC line shape is transformed into two sharp low binding energy peaks and a broader high binding energy peak. If we look at the intensity plots, these features are easily understood. The peak closest to E_F corresponds to the A band (black dots). The second sharp peak corresponds to the quasiparticle pole (B') of the B band (blue dots). The broad hump is the higher binding energy branch (B'') of the B band (red dots). The fact that the B band dispersion splits into two branches, one below (B') and one above (B'') the kink energy (blue solid line, panel (b)), is a strong coupling effect. For $\vec{k}$ values close to where B' meets the asymptote, the B' and B'' EDC features (panel (c)) comprise a true PDH structure, with the B' peak asymptotically defining the kink energy (blue dashed line). The A band feature does not develop a PDH but only sharpens upon cooling since even in the normal state it is below the kink energy for all $\vec{k}$ values in the slice. If we now move to the $\vec{k}$-value where the band crosses E_F in the normal state ($k_x = 0.19\pi$), we see only the quasiparticle peak B' (figure 2(f)).

Three spectral features similar to what we observe at $k_x = 0.1\pi$ have been reported by Feng et al. [14]. They argued that upon going superconducting, the A and B

bands both moved to lower energies and obtained more than a factor of four reduction in their energy splitting, as if the intralayer coupling $t_\perp$ was reduced in the superconducting state. Although they did not report any kink effects or any specific energy scale, they guessed that each of the low energy A and B bands should form their own PDH structure. This implies four peaks total (two peaks and two humps), although they were not able to resolve two hump structures. With the clear observation of the kink and its associated energy scale in our new work, we are able to understand their observations. First, since the normal state A band dispersion is below E_{kink} throughout this entire cut, it never develops a hump structure, while the B band develops its PDH only near where the normal state B band dispersion crosses E_{kink}. Along other cuts away from $(\pi, 0)$ the A band will disperse across E_{kink} hence developing a PDH structure, although the kink or coupling strength weakens away from $(\pi, 0)$ so this effect may never be observable. The B' peak does not extend to the $(\pi, 0)$ point as sketched by Feng et al., but rapidly dies away as spectral weight is transferred to the B'' hump. This limited momentum span is due to finite coupling, an estimate of which will be presented below. As coupling grows, more spectral weight will be transferred from B'' to B', enabling the B' dispersion to be visible over a larger momentum range.

If we now move to $k_x = 0$ on figure 2(b) and examine the EDC temperature dependence (figure 2(e)), we see that the coupling is not large enough for the B' dispersion to extend to $(\pi, 0)$. Consistent with the analysis of figure 1, we see the low energy peak of the A band $\sim 20 meV$ and broad hump corresponding to the B'' branch at $\sim 100 meV$, with no sign of the B' peak. The only signature of the kink energy scale (blue dashed line) is an increased coherence of the A band peak. Previous ARPES [3, 4, 5] and tunnelling [7] studies have attempted to relate the INS resonance energy $\Delta + \omega_R$ to the energy of the dip in the peak-dip-hump structure at $(\pi, 0)$. Figures 2(c) and (e) demonstrate that the dip energy scale (red dashed line) in general does not match the kink energy scale (blue dashed line).

To produce a strong kink in the B band dispersion and the accompanying PDH in the EDC lineshape, a fairly large coupling strength (with a dimensionless coupling constant λ of order of 1 or more) is required. The mass renormalization associated with the electronic coupling is related to the quasiparticle velocity ($\frac{1}{\hbar}\frac{dE}{dk}$), which is decreased by the factor $1 + \lambda$ below the energy scale of the kink. For example, given a coupling strength of $\lambda = 1$, the low energy dispersion will be half as steep as it is in the absence of the coupling. As the dispersion is directly measurable in ARPES, the coupling strengths are also in principle directly measurable, assuming that a "non-interacting" dispersion can be determined. For data along the nodal direction $(0,0)-(\pi,\pi)$ (figure 2(a)), where the superconducting gap goes to zero, the coupling strength has been estimated in several different

ways [19, 20]. Only a single energy band is present since bilayer splitting goes to zero here [13, 14]. One method for estimating λ is to examine the difference between the superconducting (red dots) and normal state (black dots) dispersions at low energy, which implicitly assumes that the coupling is not present in the normal state. From figure 2(a) we estimate $\lambda \sim 0.1$ using this method, consistent with the observation that the normal and superconducting state MDC dispersions are very similar [19]. An alternative way is to consider a "non-interacting" dispersion obtained by extrapolating the high energy dispersion to zero energy at k_F (black line in figure 2(a)). This method gives a coupling strength of $\lambda \sim 0.7$ for both the normal and superconducting states.

For the data of figure 2(b) at $(\pi, 0)$, the superconducting gap complicates the issue of accurately extracting λ. To estimate the "non-interacting" dispersion we might start with that expected from the Bardeen-Cooper-Schrieffer (BCS) theory. In BCS, the superconducting state dispersion is $E(\vec{k}) = \sqrt{(\epsilon(\vec{k})^2 + \Delta(\vec{k})^2)}$, where $\epsilon(\vec{k})$ is the normal state dispersion and $\Delta(\vec{k})$ is the gap. Here we use $\Delta = 18 meV$ defined as the minimum energy of the EDC peak. For $\epsilon(\vec{k})$ we use the MDC dispersion derived from the normal state data, as this data does not display any kinks (figure 1). The resulting $\epsilon(\vec{k})$ is indicated by the black line in figure 2(b). It is clear that the measured dispersion (either EDC or MDC) deviates significantly from the BCS prediction. This difference points to significant interaction effects. Focussing on the EDC dispersion near the gap edge, we see that it is significantly flatter than the calculated BCS dispersion, as if a renormalized $\epsilon(\vec{k})$ was gapped. Parameterizing the low energy portion (-18 to $-30 meV$) of the superconducting data by $E(\vec{k}) = \sqrt{\left(\frac{\epsilon(\vec{k})}{1+\lambda}\right)^2 + \Delta(\vec{k})^2}$ gives the best agreement with $\lambda = 1.05$. This analysis ignores the information contained in the strength of the kink. Preliminary analysis of the $(\pi, 0)$ kink strength in this data within the spin-fluctuation model also indicates a lambda close to 1 [26]. It also assumes that there is no coupling in the normal state, the validity of which is not clear at this time and requires further study. Instead, the lack of a kink in the normal state may be due to the energy smearing of the magnetic excitations [24]. Regardless of the details, a simple comparison of the $(\pi, 0)$ data to the nodal data in figure 2(a) indicates that the coupling effects at $(\pi, 0)$ are much stronger than they are along the node, which had previously been argued to show strong coupling [19]. Consistent with this, the normal and superconducting EDCs along the nodal direction show little observable PDH effect, as can also be seen by the absence of two dispersion branches near E_{kink} in figure 2(a). This result conflicts with earlier reports of a PDH along the nodal direction [19]. These points support the viewpoint that the electronic interactions near $(\pi, 0)$ and along $(0, 0)-(\pi, 0)$ are distinctly different in nature. We also note that this work directly contradicts the theoretical arguments of Kee et al. [25], who argue that the

electron-resonance mode coupling should have a maximal λ of order 0.05, i.e. the resonance mode should be highly irrelevant to the superconductivity. Theoretical arguments favoring a sizeable λ are contained in ref [27].
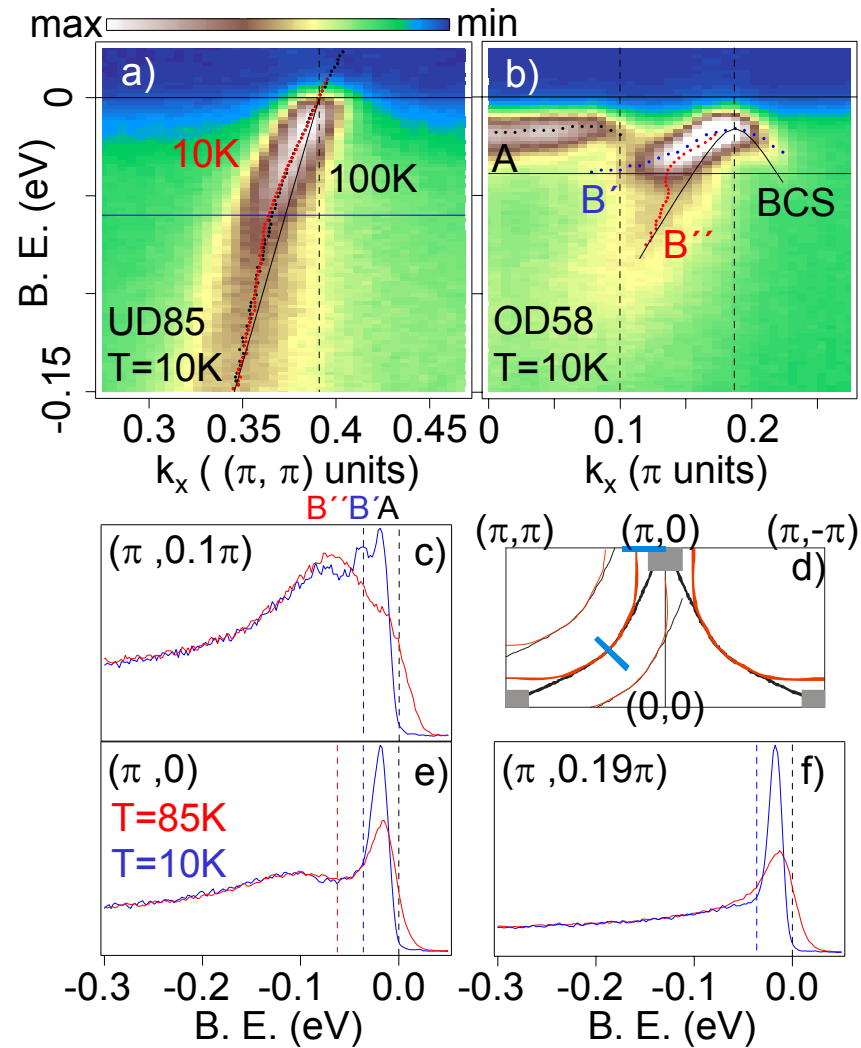
[1] J. Orenstein and A.J. Millis, Science **288**, 468 (2000).
[2] D.S. Dessau *et al.*, Phys. Rev Lett. **66**, 2160 (1991); Phys. Rev. B **45**, 5095 (1992).
[3] M.R. Norman *et al.*, Phys. Rev. Lett. **79**, 3506 (1997); Phys. Rev. B. **57**, R11089 1998.
[4] J.C. Campuzano *et al.*, Phys. Rev. Lett. **83**, 3709 (1999).
[5] A. Kaminski *et al.*, Phys. Rev. Lett. **86**, 1070 (2001).
[6] Ch. Renner and O. Fischer, Phys. Rev. B. **51**, 9208 (1995).
[7] J.F. Zasadinski *et al.*, Phys. Rev. Lett. **87**, 067005 (2001).
[8] W.L. McMillan and J.M. Rowell, in *Superconductivity*, ed. R.D. Parks (Marcel Decker, New York, 1969).
[9] C.M Varma *et al.*, Phys. Rev. Lett. **63**, 1996 (1989).
[10] P.W. Anderson, *The Theory of Superconductivity in the High-T_c Cuprates* (Princeton Univ. Press, Princeton, 1997).
[11] P.Bourges, in *The Gap Symmetry and Fluctuations in High Temperature Superconductors*, ed. J.Bok *et al.* (Plenum, Cambridge, 1998).
[12] D.L. Feng *et al.*, Science **280**, 277 (2000); H. Ding *et al.*, Phys. Rev. Lett. **87**, 227001 (2001).
[13] Y.-D. Chuang *et al.*, Phys. Rev. Lett. **87**, 177002 (2001).
[14] D.L. Feng *et al.*, Phys. Rev. Lett. **86**, 5550 (2001).
[15] A.A. Kordyuk *et al.*, cond-mat/0110379.
[16] Y.-D. Chuang *et al.*, cond-mat/0107002.
[17] H. Ding *et al.*, Nature **382**, 51 (1996); A.G. Loeser *et al.*, Science **273**, 325 (1996).
[18] A.D. Gromko *et al.*, cond-mat/0202329.
[19] A. Lanzara *et al.*, Nature **412**, 510 (2001).
[20] P.D. Johnson *et al.*, Phys. Rev. Lett. **87**, 177007 (2001).
[21] The use of both EDCs and MDCs to determine dispersion has become well accepted, with the various methods most useful in opposite regimes. In particular, the EDCs are most useful where the dispersion is very flat, e.g. for the A band dispersion and for the B band near the gap edge (figure 2(b)). On the other hand, the MDCs are most useful where the dispersion is steep, e.g. for the B band between 50 and 100 meV, as well as for the nodal data of figure 2(a).
[22] A.D. Gromko *et al.*, cond-mat/0003017.
[23] For an overview see D.J. Scalapino in *Superconductivity*, edited by R.D. Parks (Marcel Decker, New York, 1969).
[24] P. Bourges *et al.*, Nature **288**, 1234 (2000).
[25] H.-Y. Kee *et al.*, cond-mat/0110478.
[26] Ar. Abanov, A. Chubukov, and D. Pines, private communication.
[27] Ar. Abanov *et al.*, cond-mat/0112126.

FIG. 1: (a)-(j) ARPES data from OD71 at temperatures above (top row) and below (bottom row) T_c. The angular cuts are parallel to the $(\pi,\pi) - (\pi,0) - (\pi,-\pi)$ symmetry line (blue bar, panels (m,n) inset). The k_y location of each cut is labelled on each panel. (k),(l) ARPES data from OP91 above and below T_c for cuts at $k_y = 0.8\pi$. (m),(n) EDC data along the $(0,0) - (\pi,0)$ symmetry line ($k_x = 0$) for both the normal (red curves) and superconducting (blue curves) states. The inset shows the EDC locations in the 2D Brillouin zone as open (OP91) and closed (OD71) circles.

FIG. 2: (a),(b) Superconducting state ARPES data from UD85 along $(0,0) - (\pi,\pi)$ and from OD58 near $(\pi,0)$ (blue bars, panel (d)). On panel (a), the normal state MDC-derived dispersion (black dots) is plotted in addition to the superconducting state dispersion (red dots). On panel (b) the A and B band MDC and EDC dispersions are plotted as discussed in the text. (c),(e),(f) EDCs in the normal (red) and superconducting (blue) states extracted from OD58 at the labelled momentum locations, also shown as dashed lines on panel (b).
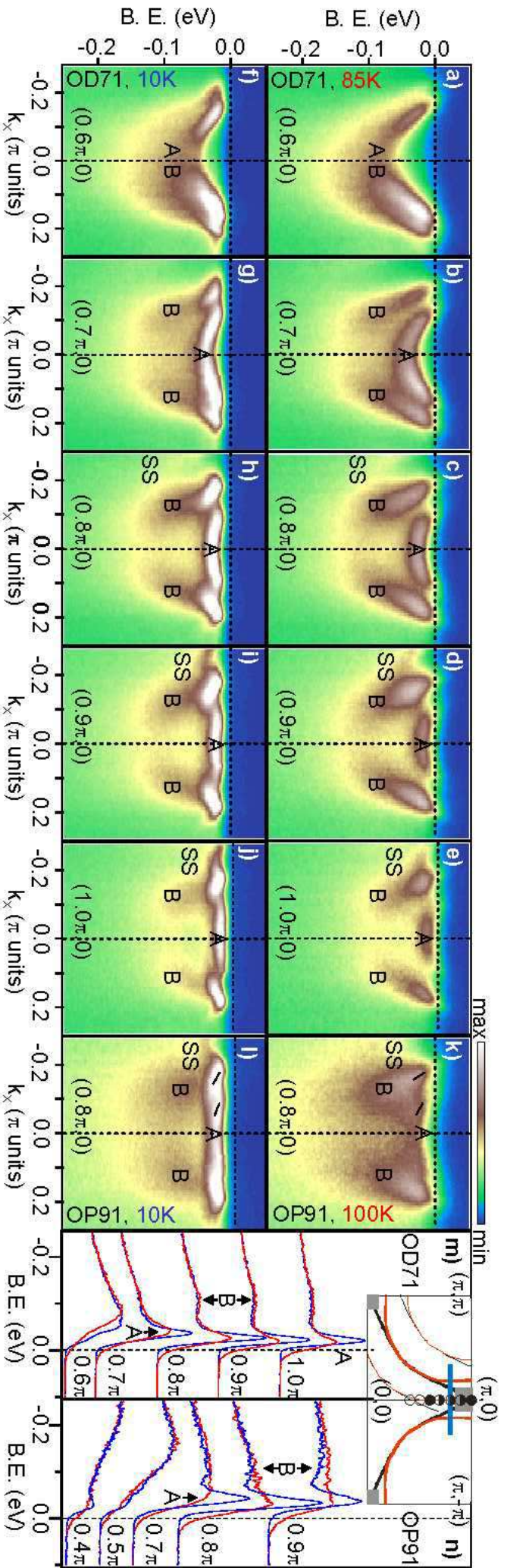
Gromko et al., Figure 1

Gromko et al., Figure 2